RSC Advances

RSC Publishing

COMMUNICATION

View Article Online
View Journal | View Issue

Synthesis of nano-$Li_4Ti_5O_{12}$ decorated on non-oxidized carbon nanotubes with enhanced rate capability for lithium-ion batteries†

Cite this: *RSC Advances*, 2013, **3**, 14267

Received 5th June 2013,
Accepted 28th June 2013

DOI: 10.1039/c3ra42759e

www.rsc.org/advances

Hyun-Kyung Kim,[a] Kwang Chul Roh,*[b] Kisuk Kang[c] and Kwang-Bum Kim*[a]

In this study, we report a facile strategy for the synthesis of $Li_4Ti_5O_{12}$ nanoparticles (15–20 nm) uniformly decorated on non-oxidized carbon nanotubes (CNTs) for use as the anode material in Li-ion batteries. In the newly designed microwave solvothermal synthesis, the CNTs were used to selectively heat a substrate for facilitating the preferential precipitation of nanoparticles. The resulting sample delivered a reversible capacity of 172 mA h g^{-1} at 1 *C*-rate and showed remarkable rate capability by maintaining 60% of the capacity at 60 *C*-rate (*vs.* 1 *C*-rate).

Introduction

Lithium-ion batteries are extensively being used as energy storage devices for electric vehicles (EV) and other portable electric devices.[1,2] However, one of the limiting safety issues is the growth of dendritic lithium on the surface of the graphite anode at high charging currents, especially at potentials approaching 0 V *versus* Li at the end of Li insertion.[2,3] This constraint could possibly be circumvented by the use of electrochemical redox couples with higher equilibrium potentials, which make Li formation thermodynamically less favourable.

Spinel $Li_4Ti_5O_{12}$ has attracted much attention as an anode material for lithium-ion batteries, because of its good Li-ion intercalation and de-intercalation reversibility and near-zero strain during charge/discharge processes.[1–3] Despite these advantages, $Li_4Ti_5O_{12}$ still lacks commercial implementation due to its low conductivity (10^{-13} S cm^{-1}), which in turn leads to initial capacity loss and poor rate capability.[2] Thus far, several effective ways, including reduction of particle size to nanoscale, doping with small amounts of metallic or non-metallic ions (V^{+5}, Cr^{3+}, Mn^{3+}, Zr^{4+}, F^-, and Br^-) in Li, Ti or O sites, surface modification and carbon coating, and formation of composite with carbonaceous materials, have been proposed for improving the rate capability of $Li_4Ti_5O_{12}$.[4–9]

In particular, reduction of $Li_4Ti_5O_{12}$ particle size to nanoscale is expected to enhance the rate capability owing to the following reasons: (1) increase in the effective interfacial area between nanosized $Li_4Ti_5O_{12}$ and the electrolyte, (2) high electrical conductivity of electrode, and (3) shorter diffusion length during the charge/discharge cycle.[10,11] However, these nanosized metal oxides have the inherent disadvantage of agglomeration, limiting their uniform dispersion in electrodes. In addition, use of large amount of binder to prevent agglomeration, in turn complicates the electrode preparation process.

To overcome these issues, it has been recently been proposed that the formation of nanocomposites of these metal oxides with carbonaceous materials will improve their electrochemical properties. Such metal oxide/carbon matrix nanocomposites are expected to facilitate the diffusion of Li ions, owing to the enhancement in their electronic conductivity and morphological stability. Additionally, dispersing the metal oxide on the carbon matrix will hinder the agglomeration of the metal oxide, providing efficient and stable framework during charge/discharge cycling.[12–14] Recently, it has been reported that the rate capability of $Li_4Ti_5O_{12}$ has been significantly improved by forming nanocomposite of $Li_4Ti_5O_{12}$ nanoparticles with nanocarbon materials using solution-based methods.[14,15] Nanocarbon materials, such as carbon nanotubes (CNTs) and reduced graphene oxide, used in the preparation of such nanocomposites effectively improved the electronic conductivity of the electrode, thereby enhancing the rate capability.[11–16]

However, the fabrication of these nanocomposite materials demand functionalized methods, such as acid-treated CNTs and

[a]*Department of Materials Science & Engineering, Yonsei University, 50 Yonsei-ro, Seodaemun-gu, Seoul 120-749, Republic of Korea. E-mail: kbkim@yonsei.ac.kr; Fax: +82-2-312-5375; Tel: +82-2-365-7745*

[b]*Energy Efficient Materials Team, Energy & Environmental Division, Korea Institute of Ceramic Engineering & Technology, 233-5 Gasan-dong, Guemcheon-gu, Seoul 153-801, Republic of Korea. E-mail: rkc@kicet.re.kr; Fax: +82-2-3282-2475; Tel: +82-2-3282-2463*

[c]*Department of Materials Science and Engineering, Seoul National University, 599 Gwanak-ro, Gwanak-gu, Seoul 151-741, Republic of Korea*

† Electronic supplementary information (ESI) available: schematic illustration of the protocol adopted for the synthesis of $Li_4Ti_5O_{12}$/CNT nanocomposite; schematic diagram of the cell used for measuring the electrical conductivity of the samples by using 2-point probe method; Raman spectrum of $Li_4Ti_5O_{12}$; SEM, TEM images and charge-discharge curves of $Li_4Ti_5O_{12}$ nanoparticles prepared in the absence of CNTs; thermogravimetric analysis (TGA) of $Li_4Ti_5O_{12}$/CNTs nanocomposite; comparison of rate capabilities for $Li_4Ti_5O_{12}$/CNTs nanocomposite. See DOI: 10.1039/c3ra42759e

graphene oxide by acid treatment or oxidation process.[14–17] Such treatments result in high density of oxygen functional groups, such as hydroxyl, carboxyl, and epoxy groups, that interact strongly with metal or metal oxide nanoparticles.[18,19] Despite subsequent thermal annealing or chemical reduction process, the defects introduced during the acid treatment or oxidation process still existed. Consequently, these led to undesirable surface defects that could degrade the electrical conductivity and mechanical stiffness of nanocarbons. Therefore, removal of residual oxygen in nanocarbon becomes very important for improving the electrical conductivity.[20,21]

Furthermore, the fabrication of these nanocomposites demanded multi-step, time-consuming processes and the use of hazardous reaction media such as strong acid or base. Such tedious synthesis methodologies generate large amount of waste, which pose potential environmental concerns. Therefore, it is of critical need to develop simple and environmentally benign synthesis strategies for the preparation of nano-$Li_4Ti_5O_{12}$ decorated on nanocarbon matrix with improved rate capability.

Herein, we report a facile process based on microwave-solvothermal synthesis, in which CNTs were used to selectively heat the substrate for facilitating the preferential precipitation of $Li_4Ti_5O_{12}$ nanoparticles (10–15 nm). Additionally, the proposed method does not involve any acid treatment or oxidation process. The $Li_4Ti_5O_{12}$/CNT nanocomposites prepared in this study exhibited excellent rate performance as an anode material for lithium-ion batteries.

Experimental

Synthesis of $Li_4Ti_5O_{12}$/CNT nanocomposite

$Li_4Ti_5O_{12}$/CNT nanocomposite was synthesized *via* simple microwave-solvothermal reaction of CNTs and titanium precursor to form TiO_2/CNT nanocomposite, followed by heat treatment in the presence of LiOH aqueous to form an intermediate Li–Ti–O/CNT nanocomposite, which was finally heat-treated in partially reducing atmosphere to form $Li_4Ti_5O_{12}$/CNT nanocomposite. Fig. S1, ESI† shows the schematic of the synthesis strategy proposed for the preparation of the $Li_4Ti_5O_{12}$/CNT nanocomposite (see ESI†).

As the first step, TiO_2/CNTs nanocomposites were prepared using commercially available multi-walled carbon nanotubes (ILJIN Nanotech Co., Ltd. South Korea) of diameter 10–15 nm, length 10–50 μm, and BET surface area of 200 $m^2\ g^{-1}$. In the typical experimental procedure, 80 mg of the multi-walled CNTs was added to 70 ml of diethylene glycol (>99%, Fluka) and sonicated for 60 min, without any additional processes such as acid treatment. The sonication process was carried out to effectively disperse CNTs in the organic solvent.[22,23] Subsequently, titanium ethoxide (0.05 ml, Aldrich), ethanol (5 ml, 99.5%), and hydrogen peroxide (5 ml, 95%) were added to the sonicated solution. The solution was then transferred to a 100 ml Teflon vessel, which was sealed and digested in a MARS-5 microwave digestion system (CEM Corporation). The reaction mixture was heated to a temperature of 210 °C within 30 min using a microwave power of 400 W, and maintained at that temperature for 30 min. After the completion of the reaction, the resulting powder (TiO_2/CNT nanocomposite) was washed several times with ethanol and distilled water, and then freeze-dried for 24 h.

Following that, 0.05 g of the as-prepared TiO_2/CNT nanocomposite was added to 50 ml of 1 M LiOH aqueous solution. The resultant solution was rapidly heated to 200 °C in a microwave-solvothermal reactor and was maintained at that temperature for 20 min to form Li–Ti–O/CNT nanocomposite. The precipitate thus obtained was washed several times with distilled water and freeze-dried for 24 h. Finally, the Li–Ti–O/CNT nanocomposite powder was heat-treated at 700 °C for 5 h in the presence of 5 wt% H_2/Ar atmosphere to obtain pure spinel $Li_4Ti_5O_{12}$. This heat treatment was carried out in a partially reducing atmosphere to inhibit the oxidation of CNTs.

Characterization methods

The crystalline phase of the prepared $Li_4Ti_5O_{12}$/CNT nanocomposite was determined by using an X-ray diffractometer (XRD, D/MAX-IIIC, Rigaku) equipped with a vertical goniometer. The XRD patterns were recorded at room temperature in the range of $10^\circ < 2\theta < 80^\circ$ at intervals of 0.04°. Transmission electron microscopy (TEM, JEM2100F, JEOL) was used to observe the morphology of the as-prepared $Li_4Ti_5O_{12}$/CNT nanocomposite powders. Raman spectroscopy (Jobin-Yvon LabRam HR) was used to characterize the structure of $Li_4Ti_5O_{12}$ in the composite. The measurements were recorded using liquid N_2-cooled CCD multichannel detector at room temperature using a conventional backscattering geometry. An argon-ion laser at a wavelength of 514.5 nm was used as the laser light source. The thermal properties of $Li_4Ti_5O_{12}$/CNT nanocomposite were determined using a thermogravimetric analyser (TGA, STA 409 PC) in air atmosphere. TGA was obtained from room temperature to 800 °C at a heating rate of 10 °C min^{-1}. The electrical conductivity was measured using the two-point probe method in a poly(methyl methacrylate) (PMMA) cell, shown schematically in Fig. S2, ESI.†[24] Hence, the $Li_4Ti_5O_{12}$/CNT nanocomposite powder was compressed under a constant pressure of 8000 psi to form of a disc/pellet, the thickness of which was measured using a digital micrometer.

Preparation of electrodes and electrochemical measurement

Electrochemical properties of the prepared $Li_4Ti_5O_{12}$/CNTs nanocomposite were investigated at room temperature, using a CR2032 coin cell with metallic lithium as the negative electrode. The working electrode consisted of a mixture of 90 wt% $Li_4Ti_5O_{12}$/CNTs nanocomposite and 10 wt% polyvinylidene fluoride (PVDF) dissolved in binder *N*-methylpyrrolidone (NMP). The slurry mixture was coated on copper foil (99.7% purity, Aldrich) and then dried at 100 °C for 24 h. Each working electrode had an area of 1 cm^2 and contained 2–3 mg of the dried slurry. The electrolyte was 1 M $LiPF_6$ dissolved in a mixture of ethylene carbonate (EC) and dimethyl carbonate (DMC) at a weight ratio of 1 : 1. The coin cells were assembled in an Ar-filled glove box using a microporous polyethylene film (Celgard 2400) as separator. Charge/discharge tests and cyclic voltammetry were performed using a potentiostat/galvanostat (VMP3, Princeton Applied Research).

Results and discussion

Fig. 1 shows the XRD patterns of pristine CNTs, TiO_2/CNT, Li–Ti–O/CNT, and $Li_4Ti_5O_{12}$/CNT nanocomposites, together with the XRD patterns corresponding to standard anatase-phase TiO_2 (JCPDS card no. 12-1272), and spinel-phase $Li_4Ti_5O_{12}$ (JCPDS card no. 49-0207) for ref. 1–3. The XRD pattern of TiO_2/CNT nanocomposite (Fig. 1(b)) prepared by microwave-solvothermal reaction was found to be consistent with that of the anatase-phase TiO_2. The XRD pattern of Li–Ti–O/CNT nanocomposite, which was formed in the intermediate step, showed rocksalt-like phase, as shown in Fig. 1(c). The origin of intermediate Li–Ti–O/CNT is discussed in detail in the following section. The XRD pattern of the prepared $Li_4Ti_5O_{12}$/CNT nanocomposite (Fig. 1(d)) matched well with the XRD pattern of standard $Li_4Ti_5O_{12}$, which confirms that the $Li_4Ti_5O_{12}$ in the $Li_4Ti_5O_{12}$/CNT nanocomposite has a pure spinel structure. Major diffraction peaks found at 2θ corresponding to 18.4°, 35.6°, 43.3°, 47.4°, 57.2°, 62.8°, and 66.1° can be attributed to respectively (111), (311), (400), (331), (511), (440), and (531) planes of a face-centred cubic spinel structure with Fd-3m space groups. The broad peak observed at around 25° corresponds to the (002) plane of the CNTs.[25] No other peaks were observed corresponding to possible impurities, such as titanium oxide or other phases of lithium titanate. The formation of phase-pure $Li_4Ti_5O_{12}$ was further confirmed by Raman spectroscopy (Fig. S3, see ESI†).[26] From the XRD data, the lattice constant of the spinel $Li_4Ti_5O_{12}$ nanoparticles in the $Li_4Ti_5O_{12}$/CNT nanocomposites was calculated to be 8.36 Å. This result was in good agreement with the lattice constant reported for pure spinel $Li_4Ti_5O_{12}$.[3]

Fig. 2 shows the TEM images of the different samples obtained during various stages of the process, namely, TiO_2/CNT nanocomposite, intermediate Li–Ti–O/CNT nanocomposite, and $Li_4Ti_5O_{12}$/CNT nanocomposite. The TEM images of the TiO_2/CNT nanocomposite prepared by microwave-solvothermal reaction (Fig. 2(a) and (b)) show that TiO_2 nanoparticles of size 3–5 nm were coated uniformly onto the CNTs. Starting from the TiO_2/CNT nanocomposite, an intermediate Li–Ti–O/CNT nanocomposite was synthesized *via* microwave-solvothermal reaction of TiO_2/CNT in an aqueous LiOH solution. The TEM image of the sample thus obtained is shown in Fig. 1(c). This reaction is believed to proceed *via* dissolution and precipitation of the metal oxide on the surface of CNTs and on the web-like network structure formed by the CNTs. Subsequently, upon annealing this sample at 700 °C for 5 h in 5 wt% H_2/Ar atmosphere, the intermediate Li–Ti–O phase gets converted to stable $Li_4Ti_5O_{12}$ nanoparticles of size 10–15 nm, as evidenced from the TEM images shown in Fig. 2(d), (e) and (f). This indicates that the heat treatment of Li–Ti–O in 5 wt% H_2/Ar atmosphere resulted in the formation of $Li_4Ti_5O_{12}$ phase, without affecting the particle size. The high-resolution TEM image shown in Fig. 2(g) clearly indicates the formation of a well-crystallized $Li_4Ti_5O_{12}$ structure with lattice fringes of *ca.* 0.48 nm corresponding to (111) interplanar spacing of $Li_4Ti_5O_{12}$.[1,2]

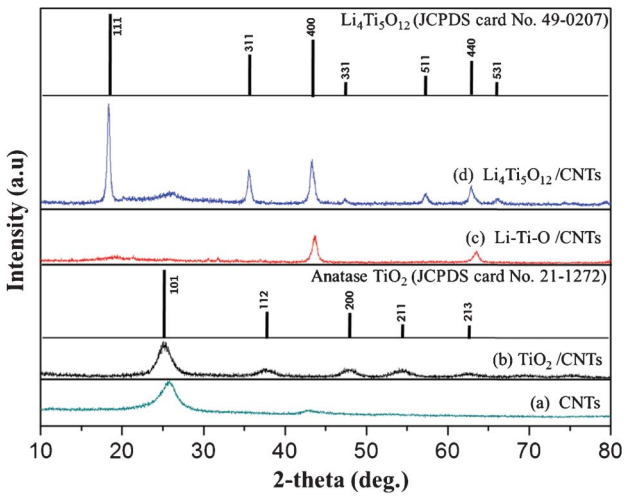

Fig. 1 XRD patterns of (a) pristine CNTs, (b) TiO_2/CNT nanocomposite, (c) (Li–Ti–O)/CNT nanocomposite, (d) $Li_4Ti_5O_{12}$/CNT nanocomposite. The XRD patterns corresponding to standard anatase-phase TiO_2 (JCPDS card no. 12-1272) and spinel-phase $Li_4Ti_5O_{12}$ (JCPDS card no. 49-0207) are provided for reference.

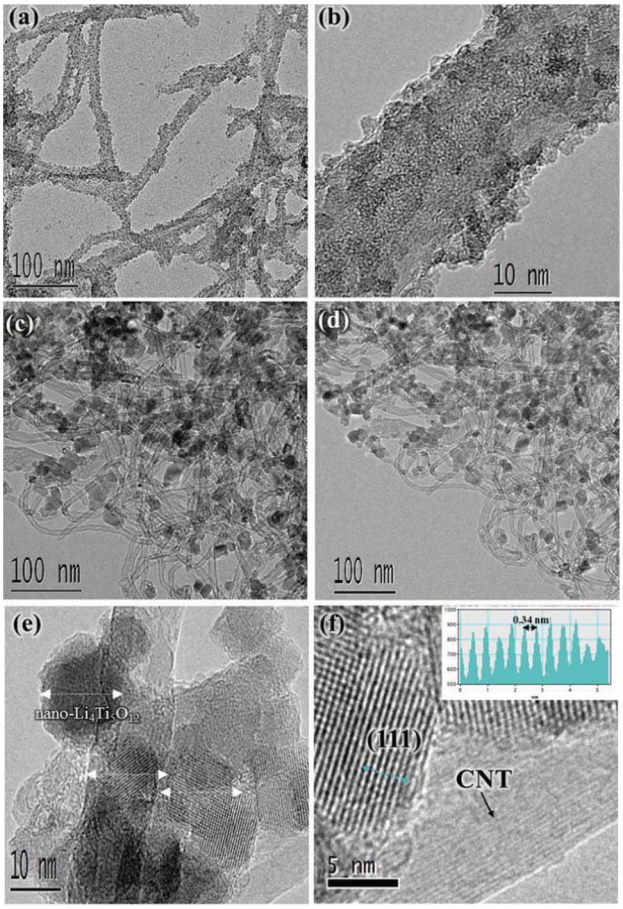

Fig. 2 TEM images of (a) and (b) TiO_2/CNT nanocomposite (particle size: 3–5 nm) synthesized using microwave-solvothermal process, (c) Li–Ti–O/CNT nanocomposite ($Li_4Ti_5O_{12}$ precursor) with a particle size of 10–15 nm obtained by lithiation of TiO_2/CNT nanocomposite, (d) and (e) $Li_4Ti_5O_{12}$/CNT nanocomposite (particle size: 10–15 nm) obtained by heat treatment of Li–Ti–O/CNT nanocomposite under partially reducing atmosphere, (f) high-resolution TEM images of the prepared $Li_4Ti_5O_{12}$/CNT nanocomposite, clearly indicating the formation of $Li_4Ti_5O_{12}$ nanoparticles of size 10–15 nm on the surface of CNTs.

Based on the detailed characterization of the samples formed during various stages of the process, the possible reaction pathway is proposed as follows. For the formation of TiO_2/CNT nanocomposite, the pristine CNTs acted as a template for the selective heterogeneous nucleation and growth of TiO_2 nanoparticles. The TiO_2/CNT nanocomposite thus obtained was reacted with LiOH solution *via* a microwave-solvothermal process, whereupon TiO_2/CNT was converted to Li–Ti–O/CNT nanocomposite. This served as the precursor for the formation of $Li_4Ti_5O_{12}$. Finally, upon heating, the Li–Ti–O/CNT nanocomposite transformed to highly crystalline phase-pure $Li_4Ti_5O_{12}$/CNT nanocomposite.

During this reaction, CNT is believed to have played two important roles: (1) The CNT matrix hindered the aggregation of $Li_4Ti_5O_{12}$ nanoparticles during the heat treatment, by preventing the interaction between adjacent $Li_4Ti_5O_{12}$ nanoparticles. This was also confirmed by preparing $Li_4Ti_5O_{12}$ nanoparticles without CNTs. In this case, the formed $Li_4Ti_5O_{12}$ nanoparticles (size < 50 nm) were highly agglomerated, as evidenced from the TEM and SEM images shown in Fig. S4 (see ESI†). (2) CNTs selectively heated the catalyst and substrate without bulk heating of the solution. In general, carbonaceous materials selectively heat the catalyst and substrate without bulk heating of the solution.[27,28] The carbonaceous materials tend to absorb microwave energy and convert it into heat, to establish high temperature on the surface of CNTs relative to the solution. Since the nucleation of metal ions occurs preferentially on hot spots, the TiO_2 or $Li_4Ti_5O_{12}$ precursor (Li–Ti–O) in solution is expected to have precipitated on the surface of the CNTs. Additionally, the microwave-solvothermal method would have favoured the process owing to its distinct advantages over conventional hydrothermal or solvothermal methods, such as lower synthesis temperature, higher reaction rate, shorter reaction time, and smaller resulting particles.[27–30]

Fig. 3(a) shows the cyclic voltammograms (CVs) of 80 wt% $Li_4Ti_5O_{12}$ loaded $Li_4Ti_5O_{12}$/CNT nanocomposite measured with potential scan rates of 0.2, 0.5, 1, 2, 5 mV s^{-1}, in the potential window of 1.0–2.5 V. The loading amount of $Li_4Ti_5O_{12}$ in the $Li_4Ti_5O_{12}$/CNT nanocomposite was evaluated to be 80 wt% from thermo-gravimetric analysis (Fig. S5, see ESI†). The CV at 0.2 mV s^{-1} clearly shows one set of well-defined current peaks at 1.50 and 1.62 V, which correspond to those of phase-pure $Li_4Ti_5O_{12}$.[1–3] Interestingly, the general shape of the CV was well maintained, even upon increasing the potential scan rate up to 2 mV s^{-1}. This suggests the good high-rate capability of the prepared $Li_4Ti_5O_{12}$/CNT nanocomposite.

Fig. 3(b) shows the charge and discharge curves of the prepared $Li_4Ti_5O_{12}$/CNT nanocomposite measured with a half-cell system using coin-cell. Charge–discharge curves were obtained between 1 and 2.5 V (*vs.* Li/Li^+) at *C*-rate of 1 to 60. The discharge curve of the $Li_4Ti_5O_{12}$/CNT nanocomposite showed the typical discharge behaviour of spinel $Li_4Ti_5O_{12}$, with a dominant plateau of 1.55 V at 1 *C*-rate. The specific discharge capacity of the second cycle based on the $Li_4Ti_5O_{12}$ weight was observed to be 172 mA h g^{-1} at 1 *C*-rate, which is close to the theoretical capacity. A specific discharge capacity of 104 mA h g^{-1} in the second cycle was achieved even at 60 *C*-rate, a value that is 60% of the 1 *C*-rate specific capacity (Fig. 3(c)). This indicates the excellent high-rate capability of the prepared $Li_4Ti_5O_{12}$/CNT nanocomposite (Fig. S6, see ESI†). Further, this result suggests that the $Li_4Ti_5O_{12}$/CNT nanocomposite perform as having perfect ionic and electric paths.

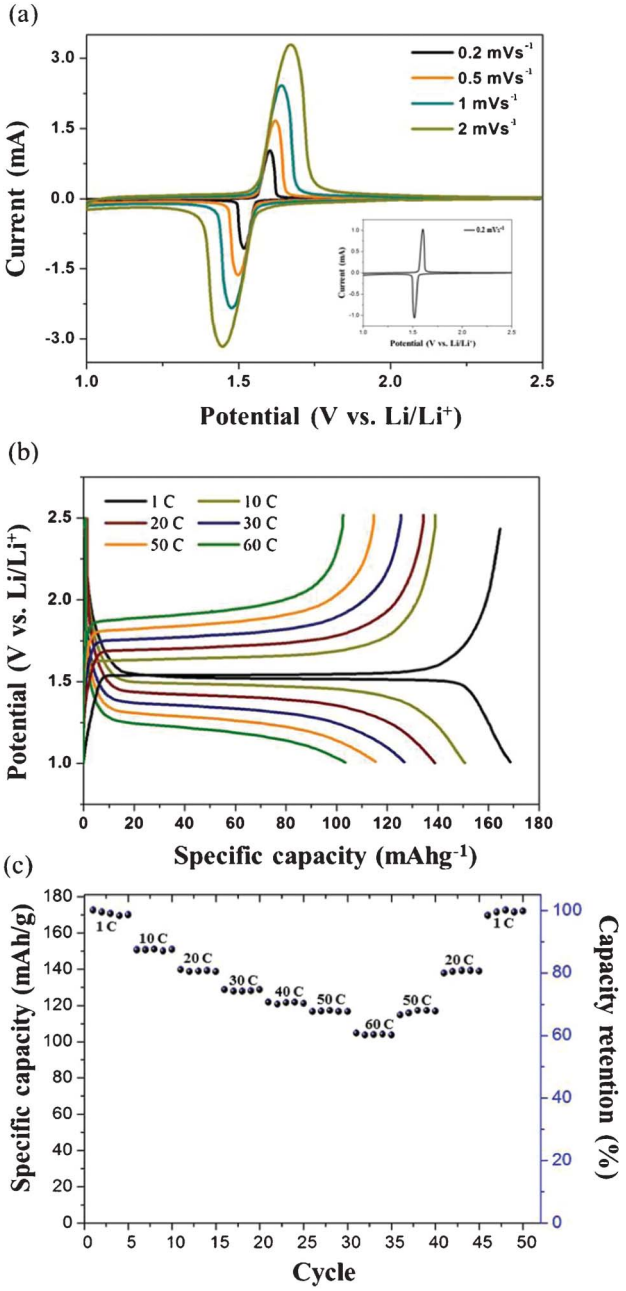

Fig. 3 (a) Cyclic voltammograms (CVs) of 80 wt% $Li_4Ti_5O_{12}$ loaded $Li_4Ti_5O_{12}$/CNT nanocomposite under different scan rates: 0.2, 0.5, 1, and 2 mV s^{-1}. (b) Second charge–discharge curves of $Li_4Ti_5O_{12}$/CNT nanocomposite half-cell, showing its rate capability under different current rates (from right to left): 1, 10, 20, 30, 50, and 60 *C*-rate. (c) Plot of capacity retention *versus* different rates (1, 10, 20, 30, 50, and 60 *C*-rate), where 1 *C*-rate corresponds to a current density of 172 mA g^{-1}.

The observed significant improvement in the rate capability could be attributed to the synthesis of $Li_4Ti_5O_{12}$/CNTs nanocomposite with the following features: (1) nanosized $Li_4Ti_5O_{12}$ particles providing shorter diffusion length and (2) uniform distribution/

decoration of $Li_4Ti_5O_{12}$ nanoparticles onto the surface of the non-oxidized CNTs. In general, smaller particles promote shorter pathways for the solid-state diffusion of Li ions. Hence, the nanoscale dimension of the prepared $Li_4Ti_5O_{12}$ particles resulted in a better rate capability. In addition, the uniform dispersion of $Li_4Ti_5O_{12}$ nanoparticles on the surface of non-oxidized CNTs and in the web-like network structure could have improved the electrical conductivity of the electrode, and acted as a good additive to disperse nano-$Li_4Ti_5O_{12}$ by connecting them with a 1-D conduction path. This was experimentally verified by measuring the electrical conductivity of the prepared $Li_4Ti_5O_{12}$/CNTs nanocomposite by using the two-point probe method. The schematic of the cell and the compressed pellet used for measuring the electrical conductivity is shown in Fig. S2 in the ESI.† It was found that the electrical conductivity of the $Li_4Ti_5O_{12}$/CNT nanocomposite (1.88 S cm^{-1}) was relatively lower when compared to that of pristine CNTs (5 S cm^{-1}). Nevertheless, the electrical conductivity of the $Li_4Ti_5O_{12}$/CNT nanocomposite was much higher than that of pure $Li_4Ti_5O_{12}$ (10^{-13} S cm^{-1}).[1–3] This confirms that the CNTs enhance the electrical conductivity of $Li_4Ti_5O_{12}$.

Furthermore, the cyclability of the prepared composite was analysed. It was found that the $Li_4Ti_5O_{12}$/CNT nanocomposite exhibited excellent capacity retention of 97% at 1 *C*-rate over 200 cycles and 98% at 10-C rate over 1000 cycles, as shown in Fig. 4(a) and (b). In addition, the Coulombic efficiency remained at about 100%, demonstrating the excellent cycling performance of the $Li_4Ti_5O_{12}$/CNT nanocomposite. Additionally, post-cycling characterization of the composite was performed to understand the volumetric expansion of $Li_4Ti_5O_{12}$ during charge–discharge cycling. For this, a sample tested for several the cycles was broken down and analysed using TEM. The TEM images of $Li_4Ti_5O_{12}$/CNT nanocomposite after electrochemical cycling (Fig. 4(c)) indicated the presence of $Li_4Ti_5O_{12}$ nanoparticles, CNTs, and binders. After electrochemical cycling, the $Li_4Ti_5O_{12}$ particles showed new features in TEM that are due to diffraction contrast. Other than that, almost all the $Li_4Ti_5O_{12}$ nanoparticles in $Li_4Ti_5O_{12}$/CNT composite appear to be relatively unchanged. These $Li_4Ti_5O_{12}$ nanoparticles are distributed uniformly on the surface of the CNTs.

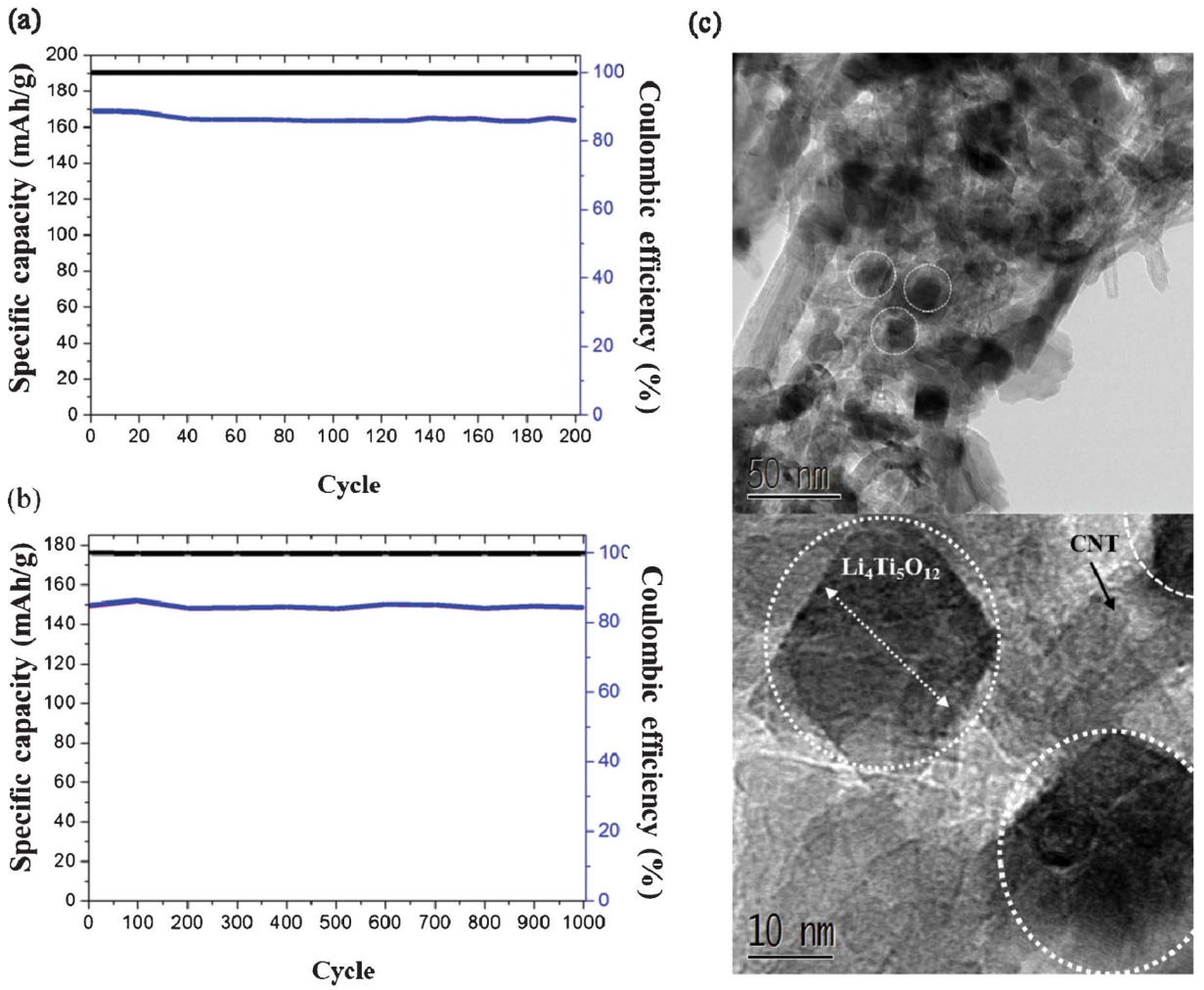

Fig. 4 Cyclability of $Li_4Ti_5O_{12}$/CNT nanocomposite at (a) 1 *C*-rate over 200 cycles (b) 10 *C*-rate over 1000 cycles, (c) TEM images of $Li_4Ti_5O_{12}$/CNT nanocomposite after electrochemical cycling, indicating the presence of $Li_4Ti_5O_{12}$ nanoparticles, CNT, and binders.

Conclusions

$Li_4Ti_5O_{12}$/CNT nanocomposites were successfully synthesized by a microwave-solvothermal reaction and post-heat treatment without any hazardous reaction media, such strong acid or base. The TEM image of the prepared composite shows the formation of $Li_4Ti_5O_{12}$ nanoparticles of size 10–15 nm uniformly decorated on CNTs. The specific discharge capacity of the second cycle based on the $Li_4Ti_5O_{12}$ weight was 172 mA h^{-1} at 1 *C*-rate and 104 mA h^{-1} even at 60 *C*-rate, which is 60% of the capacity at 1 *C*-rate. This indicates the excellent high rate capability of the prepared nanocomposite. In addition, the $Li_4Ti_5O_{12}$/CNT nanocomposite showed excellent rate performance as an anode electrode material in lithium ion battery system, due to the shorter diffusion length of the nanosized $Li_4Ti_5O_{12}$ uniformly formed on the non-oxidized CNTs. Furthermore, the use of non-oxidized CNTs improved the electrical conductivity of the electrode and acted as good additives to disperse nano-$Li_4Ti_5O_{12}$, connecting them with a 1-D conduction path.

Acknowledgements

This work was supported by the energy efficiency and resources of the Korea Institute of Energy Technology Evaluation and Planning (KETEP) grant funded by the Ministry of Knowledge Economy, Korean government (No: 20122010100140 and No: 2010201010006).

Notes and references

1 K. S. Park, A. Benayad, D. J. Kang and S. G. Doo, *J. Am. Chem. Soc.*, 2008, **130**, 14930.
2 H. K. Kim, S. M. Bak and K. B. Kim, *Electrochem. Commun.*, 2010, **12**, 1768.
3 H. Jung, S. Myung, C. Yoon, S. Son, K. Oh, K. Amine, B. Scrosati and Y. Sun, *Energy Environ. Sci.*, 2011, **4**, 1345.
4 G. N. Zhu, H. J. Liu, J. H. Zhuang, C. X. Wang, Y. G. Wang and Y. Y. Xia, *Energy Environ. Sci.*, 2011, **4**, 4016.
5 S. Huang, M. Woodson, R. Smalley and J. Liu, *Nano Lett.*, 2004, **4**, 2015.
6 H. M. Xie, R. S. Wang, J. R. Ying, L. Y. Zhang, A. F. Jalbout, H. Y. Yu, G. L. Yang, X. M. Pan and Z. M. Su, *Adv. Mater.*, 2006, **18**, 2609.
7 K. Naoi, S. Ishimoto, Y. Isobe and S. Aoyagia, *J. Power Sources*, 2010, **195**, 6250.
8 J. Huang and Z. Jiang, *Electrochim. Acta*, 2008, **53**, 7756.
9 B. Li, C. Han, Y. He, C. Yang, H. Du, Q. Yang and F. Kang, *Energy Environ. Sci.*, 2012, **5**, 9595.
10 C. Jiang, M. Ichihara, I. Honmaa and H. Zhou, *Electrochim. Acta*, 2007, **52**, 6470.
11 H. M. Shen, X. G. Zhang, Y. K. Zhou and H. L. Li, *Mater. Chem. Phys.*, 2002, **78**, 437.
12 K. Naoi, S. Ishimoto, Y. Isobe and S. Aoyagia, *J. Power Sources*, 2010, **195**, 6250.
13 Y. Shi, L. Wen, F. Li and H. M. Cheng, *J. Power Sources*, 2011, **196**, 8610.
14 B. Zhang, Y. Liu, Z. Huang, S. Oh, Y. G. Yu, Y. W. Mai and J. K. Kim, *J. Mater. Chem.*, 2012, **21**, 761.
15 Y. Tang, F. g. Huang, W. Zhao, Z. Liua and D. Wana, *J. Mater. Chem.*, 2012, **22**, 11257.
16 L. Shen, C. Yuan, H. Luo, X. Zhang, S. Yang and X. Lu, *Nanoscale*, 2011, **3**, 572.
17 L. Shen, C. Yuan, H. Luo, X. Zhang, K. Xua and F. Zhang, *J. Mater. Chem.*, 2011, **130**, 14930.
18 Y. Liang, D. Wu, X. Feng and K. Mullen, *Adv. Mater.*, 2009, **21**, 1679.
19 H. Wang, H. S. Casalongue, Y. Liang and H. J. Dai, *J. Am. Chem. Soc.*, 2010, **132**, 7472.
20 Y. Zhu, S. Murali, W. Cai, X. Li, J. W. Suk, J. R. Potts and R. S. Ruoff, *Adv. Mater.*, 2010, **22**, 3906.
21 M. Cheng, R. Yang, L. Zhang, Z. Shi, W. Yang, D. Wang, G. Xie and D. Shi, *Carbon*, 2012, **50**, 2581.
22 J. Liu, A. G. Rinzler, H. Dai, J. H. Hafner, R. K. Bradley, P. J. Boul, A. Lu, K. Shelimov, C. B. Huffman, F. Rodriguez-Macias, Y. S. Shon, T. R. Lee, D. T. Colbert and R. E. Smalley, *Science*, 1998, **280**, 1253.
23 Y. Y. Huang and E. M. Terentjev, *Polymers*, 2012, **4**, 275.
24 S. H. Park, S. M. Bak, K. H. Kim, J. P. Jegal, S. I. Lee, J. Lee and K. B. Kim, *J. Mater. Chem.*, 2011, **21**, 680.
25 G. Maurin, C. H. Bousquet, F. Henn, P. Bernier, R. Almairac and B. Simon, *Chem. Phys. Lett.*, 1999, **312**, 14.
26 S. Huang, Z. Wen, X. Zhu and X. Yang, *J. Electrochem. Soc.*, 2005, **152**, A1301.
27 M. Tsuji, M. Kubokawa, R. Yano, N. Miyamae, T. Tsuji, M. S. Jun, S. Hong, S. Lim, S. H. Yoon and I. Mochida, *Langmuir*, 2007, **23**, 387.
28 F. Langa, P. De La Cruz, E. Espildora, J. J. Garcia, M. C. Perez and A. De La Hoz, *Carbon*, 2000, **38**, 1641.
29 A. Phuruangrat, D. J. Ham, S. J. Hong, S. Thongtem and J. S. Lee, *J. Mater. Chem.*, 2010, **20**, 1683.
30 G. J. Wilson, A. S. Matijasevich, D. R. G. Mitchell, J. C. Schulz and G. D. Will, *Langmuir*, 2006, **22**, 2016.

